

A Photometric Diagnostic to Aid in the Identification of Transiting Extra-Solar Planets

Brandon Tingley and Penny D. Sackett

*Research School of Astronomy and Astrophysics, and
Planetary Science Institute,*

*The Australian National University, Mount Stromlo Observatory, Cotter Road,
Weston, Canberra ACT 2611, Australia*

ABSTRACT

One of the obstacles in the search for exoplanets via transits is the large number of candidates that must be followed up, few of which ultimately prove to be exoplanets. Any method that could make this process more efficient by somehow identifying the best candidates and eliminating the worst would therefore be very useful. Seager & Mallén-Ornelas (2003) demonstrated that it was possible to discern between blends and exoplanets using only the photometric characteristics of the transits. However, these techniques are critically dependent on the shape of the transit, characterization of which requires very high precision photometry of a sort that is atypical for candidates identified from transit searches. We present a method relying only on transit duration, depth, and period, which require much less precise photometry to determine accurately. The numerical tool we derive, the exoplanet diagnostic η , is intended to identify the subset of candidates from a transit search that is most likely to contain exoplanets, and thus most worthy of subsequent follow-up studies. The effectiveness of the diagnostic is demonstrated with its success in separating modeled exoplanetary transits and interlopers, and by applying it to actual OGLE transit candidates.

Subject headings: (stars:) planetary systems

1. Introduction

One of the fundamental problems in the search for exoplanets via transits is the relatively small fraction of systems exhibiting periodic transits that are found to be caused by exoplanets after follow-up observations reveal the nature of the orbiting body. The process of verification consumes a great deal of telescope time on top-class instruments. This process

would be made more efficient by the development of a method that could identify the best and worst candidates from the collection of blends, binaries and exoplanets that comprise a typical candidate set from transit searches. Seager & Mallén-Ornelas (2003) touched on this possibility while exploring the feasibility of estimating stellar parameters from the photometric properties of an observed transit. Using a fully analytical derivation, they showed that four parameters (depth, period, full transit duration, and duration minus ingress and egress times) could be used to calculate physical parameters such as mean stellar density and radius ratio for the system, assuming that the transiting body is an exoplanet and that the orbit is circular. Non-planetary transiting bodies will produce somewhat aphysical parameters, particularly in the radius of the transiting body. A typical blend, for example, would produce a radius for the transiting body that would be 20%-50% larger than that expected for a close-in giant planet.

Unfortunately, this technique requires extremely precise photometry. Seager & Mallén-Ornelas quote a need for 5 millimag precision with 5 minute sampling for two transits (provided these two transits define the true period) for short-period giant planets. Current transit search campaigns do not produce data of this quality, which limits the applicability of this technique.

However, as we show, it is still possible to use the photometric properties of transits derived from less precise data to identify the best exoplanet candidates from a large sample. By using a set of reasonable approximations, we derive a numerical tool (called the exoplanet diagnostic) that indicates how “planet-like” a particular event is using only the transit period, duration and depth. This diagnostic makes it possible to exclude many of the candidates from transit searches without the need for follow-up observations, including many of those caused by blends.

In Section 2, we derive the exoplanet diagnostic and discuss the impact of orbital eccentricity. In Section 3, the results of our analysis of existing transit searches and of the effectiveness of the diagnostic in distinguishing modeled blends is presented

2. Derivation of the Exoplanet Diagnostic η

The duration, D , of a transit depends on many parameters: the radii and masses of the two transiting objects, semi-major axis, orbital inclination, eccentricity, viewing orientation and period. A completely general equation describing the duration of the transit can be derived from these variables. We begin with the derivation of transit duration given by Sackett (1999),

$$D = \frac{\Delta\phi}{\omega_t} = \frac{\Delta\phi r_t}{v_t} \quad , \quad (1)$$

in which $\Delta\phi$ is the eccentric angle between the first and last contacts of the transit, ω_t is the angular velocity of the planet at the time of the transit, r_t is the separation between the planet and the parent star at the time of transit, and v_t is the orbital velocity at this time. Assuming that r_t does not change appreciably during transit, and that $r_t \gg R_\star$ (see Fig. 1b), $\Delta\phi$ can be written as

$$\Delta\phi = \arcsin \left(2 \sqrt{\frac{(R_1 + R_2)^2}{r_t^2} - \cos^2 i} \right) \approx 2 \sqrt{\frac{(R_1 + R_2)^2}{r_t^2} - \cos^2 i} \quad , \quad (2)$$

where R_1 and R_2 are the radii of the transiting bodies and i is the orbital inclination. Invoking conservation of angular momentum L ,

$$L = \mu \sqrt{GM_{\text{tot}} a(1 - e^2)} = \mu v_t r_t \quad , \quad (3)$$

where M_{tot} is the total mass of the system, $\mu \equiv (m_1 m_2)/M_{\text{tot}}$ is the reduced mass, a is the semi-major axis of the orbit, and e is the orbit eccentricity. Putting these pieces together yields:

$$D = \frac{2(R_1 + R_2) r_t}{\sqrt{GM_{\text{tot}} a(1 - e^2)}} \sqrt{1 - \frac{r_t^2 \cos^2 i}{(R_1 + R_2)^2}} \equiv \frac{2(R_1 + R_2) r_t}{\sqrt{GM_{\text{tot}} a(1 - e^2)}} Z \quad , \quad (4)$$

where we have absorbed the geometrical effects of the projected inclination into Z . The quantity Z at most unity (in the case of an $i = 90^\circ$ central transit) and increasingly less than unity for increasing degrees of misalignment (see Fig. 2). In order to eliminate a and r_t , we invoke Kepler's third law,

$$a = \left(\frac{GM_{\text{tot}} \tau^2}{4\pi^2} \right)^{\frac{1}{3}} \quad , \quad (5)$$

where τ is the period of the orbit. Then, recalling the equation for an ellipse

$$r_t = \frac{a(1 - e^2)}{1 + e \cos \phi_t} \quad , \quad (6)$$

where ϕ_t is the eccentric angle at transit center of the system, relative to the semi-major axis of the orbit (ϕ_t depends only on viewing geometry; see Fig. 1a), we can write the final equation for the transit duration as

$$D = 2Z(R_1 + R_2) \frac{\sqrt{1 - e^2}}{1 + e \cos \phi_t} \left(\frac{\tau}{2\pi GM_{\text{tot}}} \right)^{\frac{1}{3}} . \quad (7)$$

This equation is general; in the case of exoplanets, $M_{\text{tot}} \approx M_\star$, the mass of the parent star.

2.1. Circular Exoplanetary Orbits

As there are a large number of unknowns, we first examine the simplest case of circular ($e = 0$) orbits. This is a relevant case since transit searches are most sensitive to "hot Jupiters" (that is, Jovian-mass planets with $a \leq 0.1$ AU), all of which discovered thus far have very low eccentricities. For $e = 0$ and $M_{\text{tot}} = M_\star$, Eq. 7 reduces to

$$D = 2Z(R_p + R_\star) \left(\frac{\tau}{2\pi GM_\star} \right)^{\frac{1}{3}} \quad (8)$$

where R_p is the radius of the exoplanet and R_\star is the radius of the parent star. This contains four unknowns that cannot be observed directly: Z , R_p , R_\star and M_\star . However, as we show below, it is possible to replace all but one of these with observable quantities.

Through extensive modeling of planetary transits using a standard ZAMS and limb darkening from Claret (2000) for many different exoplanet-star size ratios and projected inclinations, we find that the fractional depth d of a central exoplanetary transit in the I passband can be approximated as

$$d \approx 1.3 \left(\frac{R_p}{R_\star} \right)^2 . \quad (9)$$

Off-center transits will have only slightly lower constants of proportionality unless they are grazing, which is an unlikely, but still possible, scenario.

The mass-radius relationship for the lower main sequence (Cox 2000) proposes:

$$M_\star \approx M_\odot \left(\frac{R_\star}{R_\odot} \right)^{1.25} . \quad (10)$$

With these three equations, we create a diagnostic η , namely the ratio of the theoretical duration D (derived above) and the observed duration, D_{obs} (obtained from photometric observations). There are still unknowns: the factor Z , known to be constrained to lie between 0 and 1, and one of R_* or R_p . The latter duality leads to two different forms of the exoplanet diagnostic, η_p and η_* , each of which is useful in different circumstances.

Radii of stars that are thought to have a reasonable chance of harboring an exoplanet, namely main sequence spectral types F through late K, can vary by a factor of three or so, while the typical planetary radius that can produce a detectable transit from ground varies by about a factor of two. Therefore, ground-based transit searches would be better served by a diagnostic (η_p) that takes the unknown R_p to be constant, while satellite missions, which are sensitive to a much wider range of R_p , would be better served using a diagnostic (η_*) that assumed R_* was constant. We stress, however, that for any primaries for which the radius can be estimated (from spectral classification, for example), η_* should be used. These two exoplanet diagnostics, easily derivable from the above equations, are:

$$\eta_p \equiv \frac{D_{\text{obs}}}{D} = \frac{D_{\text{obs}}}{2Z \left(1 + \sqrt{1.3/d}\right)} \left(\frac{2\pi GM\odot}{\tau}\right)^{\frac{1}{3}} R_p^{-\frac{7}{12}} R_{\odot}^{-\frac{5}{12}} \left(\frac{1.3}{d}\right)^{\frac{5}{24}} \quad (11)$$

and

$$\eta_* \equiv \frac{D_{\text{obs}}}{D} = \frac{D_{\text{obs}}}{2Z \left(1 + \sqrt{d/1.3}\right)} \left(\frac{2\pi GM\odot}{\tau}\right)^{\frac{1}{3}} R_*^{-\frac{7}{12}} R_{\odot}^{-\frac{5}{12}} \quad . \quad (12)$$

Note that η_p is independent of R_* and η_* is independent of R_p . The one remaining unknown left in these equations, Z , will not critically affect the viability of these diagnostics. In what follows, we take $Z = 1$ and describe the consequences of this assumption.

Looking at Eqs. 4 and 7, one would expect the typical binary transit to last longer than the typical exoplanet transit, as the radius of a transiting star would far exceed that of a transiting planet, unless it was an extreme grazing eclipse. The $R_p + R_*$ for an exoplanetary transit becomes $R_{*,1} + R_{*,2}$ for a stellar eclipsing binary – a large increase in this term.

A more in-depth examination of these diagnostics gives greater insight into the situation. η_p scales as

$$\eta_p \propto D_{\text{obs}} d^{\frac{7}{24}} R_p^{-\frac{7}{12}} \tau^{-\frac{1}{3}} \quad . \quad (13)$$

while η_* scales as

$$\eta_* \propto D_{\text{obs}} \left(1 - \sqrt{\left(\frac{d}{1.3} \right)} \right) R_*^{-\frac{7}{12}} \tau^{-\frac{1}{3}} . \quad (14)$$

Decreasing the inclination of the orbit not only reduces the measured duration, D_{obs} , but also reduces the transit depth, d . Both factors act to reduce η_p , while they counteract each other for η_* . The latter has a much stronger dependence on D_{obs} than d for the shallow events that are of interest, so decreasing Z also decreases η_* . Following this line of reasoning, the diagnostics will therefore be a maximum for central transits (with $Z = 1$) and less for more grazing transits. Thus, true exoplanetary events would have a diagnostic less than or equal to one, while stellar events (blends or grazing binaries) would often, but not always, have diagnostics greater than one.

Some grazing stellar binaries and blended eclipsing binaries will have similar diagnostics to exoplanets, which will lead to some stellar contamination in the reduced set of candidates even after the diagnostic has been applied. Some grazing binaries can be identified via a clearly V-shaped transit (Udalski et al. 2002a), the presence of ellipsoidal variations (Drake 2003; Sirk & Paczyński 2003), or by virtue of the existence of a detectable secondary transit that has a different depth than that of the primary transit. Also, binary systems in which both stars are nearly identical will have a photometric period that is one-half the actual period, as it will have two identical transits per orbit. Because of this, their diagnostics are increased by a factor of $2^{\frac{1}{3}}$, helping to push them out of the regime populated by exoplanetary events. Additionally, a large percentage of systems involving transits of giant stars could in theory be identified as non-planetary, as their large radii lead to very long transit durations.

The exoplanet diagnostic should also be useful in separating most blends from exoplanetary transits. Blended eclipsing binaries would have a high $R_{*,1} + R_{*,2}$ compared to exoplanets and the dilution of their transits to a shallower depth by a third component means that their transits would generally be more central than a grazing binary for a given transit depth. They would thus have a longer duration (and a higher exoplanet diagnostic) relative to other events with a similar transit depth, whether they be grazing binaries or exoplanets. This is potentially very useful for missions such as Kepler, which will likely identify large numbers of objects that exhibit periodic transits of a variety of depths – many of which will be blends. The shallowest events are both the most interesting and the most difficult to confirm via follow-up observations; any technique that can eliminate some of these without follow-up will save significant astronomical resources.

2.2. Elliptical Exoplanetary Orbits

A good fraction of the exoplanets that have been discovered to date have nearly circular orbits. In fact, the average eccentricity for all known exoplanets with periods less than about 60 days is approximately 0.1. However, the majority has periods longer than 60 days, where the average eccentricity rises sharply to 0.3 (Halbwachs et al. 2004). We are thus led to consider the effect of eccentricity on the diagnostic. As can be seen from Eq. 7, the diagnostic depends on the eccentricity in the following fashion:

$$\eta \propto \frac{D_{\text{obs}}}{D_{\text{circ}}} = \frac{\sqrt{1-e^2}}{1+e \cos \phi_t} \quad (15)$$

The dependence on the viewing angle ϕ_t creates a distribution in the possible diagnostics for a given period and eccentricity given by:

$$S_1(\eta) = \frac{d\phi_t}{d\eta} = \frac{d}{d\eta} \left(\arccos \left(\frac{\sqrt{1-e^2} - \eta}{e\eta} \right) \right) = \frac{(1-e^2)^{\frac{1}{4}}}{\eta} \left(2\eta - (1+\eta^2)\sqrt{1-e^2} \right)^{-\frac{1}{2}}. \quad (16)$$

However, the probability that a transit will be observed to occur is inversely proportional to r_t (Sackett 1999). This means that transits are more likely to occur when r_t is smaller, the orbital velocities are correspondingly higher, and thus transit durations are correspondingly shorter. This selection effect skews the spread in observed η toward lower diagnostics (see Fig. 3):

$$S_2(\eta) = \frac{S_1(\eta)}{r_t} \propto a^{-1} \eta^{-2} \sqrt{1-e^2} \left(2\eta - (1+\eta^2)\sqrt{1-e^2} \right)^{-\frac{1}{2}}, \quad (17)$$

where we have used Eq. 15 and Eq. 6 to describe r_t in terms of η . The average η that can be expected is then:

$$\langle \eta \rangle = \frac{\int_{n_{\min}}^{n_{\max}} \eta S_2(\eta) d\eta}{\int_{n_{\min}}^{n_{\max}} S_2(\eta) d\eta} = \sqrt{1-e^2} \quad (18)$$

where $n_{\max} = \frac{\sqrt{1-e^2}}{1-e}$ and $n_{\min} = \frac{\sqrt{1-e^2}}{1+e}$, as defined by Eq. 15. Thus, we can expect the average observed η to decrease with increasing eccentricity. Unfortunately, the same is also true for binary stars, which increases the chance of a non-planetary system producing a planet-like diagnostic.

3. Putting the Diagnostic to the Test

We now illustrate the effectiveness of the diagnostic η in separating exoplanetary-like transit candidates from a large fraction of the pretenders that may be caused by eclipsing binary stars, which are either grazing or heavily blended.

3.1. Actual Transit Candidates

The transit candidates discovered by the OGLE group (Udalski et al. 2002a,b,c, 2003, 2004) provide an excellent opportunity to test the performance of the exoplanet diagnostic. Orbital periods, transit durations and depths for 137 candidates are available, along with a short list of confirmed exoplanets in the sample. The results of the application of the exoplanet diagnostic (η_p) to the OGLE candidates are shown in Fig. 4 (and the data used to create it are found in Table 1). We have assumed a planetary radius of $1R_J$, as representative of the largest hot Jupiters found. For comparison, modeled central transits of Jupiter and Saturn and the actual transit data of HD209458 (Brown et al. 2001) and trES-1 (Alonso et al. 2004) are included.

Of those OGLE candidates that have been followed up with further observations (OGLE-TR-59 and lower), OGLE-TR-56 (Konacki et al. 2003) and OGLE-TR-10 (Bouchy et al. 2004) are the only two confirmed exoplanets in this sample. Indeed, OGLE-TR-10 was confirmed after we identified it as interesting from our diagnostic analysis. They have the lowest and fifth lowest exoplanet diagnostics, respectively. The exoplanets that have been identified in the later sample (OGLE-TR-111 (Pont et al. 2004), OGLE-TR-113 and OGLE-TR-132 (Bouchy et al. 2004)), which has not been studied completely (OGLE-TR-60 and higher), are also among those with the lowest diagnostics. The modeled Jupiter and Saturn also produce low diagnostics, as do HD209458 (Brown et al. 2001) and TrES-1 (Alonso et al. 2004). This evidence makes a strong argument that our diagnostic can effectively identify candidates that are more likely to be exoplanets. As such, it seems likely that other exoplanets will be discovered in this second set of OGLE candidates. Additionally, our analysis suggests that several OGLE candidates warrant (see Table 1) a more thorough investigation, while other disputed events, such as OGLE-TR-33, do not. We note, in fact, that the most recent research suggests that OGLE-TR-33 is in fact a blend (Torres et al. 2004).

3.2. Modeled Blended Stellar Binaries

Testing the response of the exoplanet diagnostic to blended eclipsing binary systems is not as simple. In order to get an accurate impression of the events that could be observed to mimic exoplanetary transits, many different types of binary systems must be modeled at a variety of projected inclinations. The types of exoplanets that could be observed must also be modeled. Both of these tasks can be readily performed using the expectations from a standard zero-age main sequence (ZAMS) and limb darkening laws – in this case, we used those from Claret (2000). The blends can then be constructed using the modeled binary star transits and the equations for blends described by Tingley (2003). Using η_* , the diagnostics of modeled blends can be compared to those of modeled exoplanets.

Other methods may be used to eliminate blends. For example, blends will have V-shaped transits or secondary transits that would be readily identifiable in the light curves. As with grazing binaries, blends can also have primary and secondary transits of almost the same depth, again leading to an erroneous period and an increased exoplanet diagnostic. In what follows, we ignore these effects, concentrating on information from the diagnostic alone, and assuming circular orbits.

Figures 5-7 show how the diagnostic η_* evolves for blends compared to exoplanets for a variety of assumptions and conditions. The modeled blends are created by combining modeled light curves of blends and adding the proper amount of light from the ‘primary’ (the constant, brighter component for blends and the parent star for exoplanets) to create a transit of the desired depth. These figures are designed to illustrate the overall effectiveness of the diagnostic under different conditions. When studying these figures, it is important to remember that the spectral type of the primary component of a blend has nothing to do with the spectral type of the eclipsing component – it only provides photons to make the observed transits shallower.

Figure 5 shows how the diagnostic η_* evolves for blends relative to exoplanets for different spectral types and transit percentages, assuming that nothing is known about the ‘primary’ and therefore using $R_* = R_\odot$ when calculating η_* . The lines help to illustrate the likelihood of finding a blends with the listed spectral type and transit percentage that have similar diagnostic to exoplanets. The shaded regions show what diagnostics exoplanets with radii from $1.5R_J$ (right boundary) to R_{Mercury} (left boundary) and transit percentages from 0% (top) to 75% (bottom) would produce if the ‘primary’ was an F2 star (angled 45° to the right), a Solar-type star (horizontal dotted lines) and an M3 star (angled 45° to the left). Unblended binaries occupy the right-hand end of each line. From this figure, it is clear that in most cases, even without any knowledge of the ‘primary’, most blends are distinguishable from exoplanets in the case of circular orbits, even for exoplanets smaller than Earth. This

is especially true for blends involving earlier-type eclipsing binaries, as those tend to have relatively long transits.

Figure 6 shows how η_* is influenced specifically by the spectral type of the binary in the blend for different transit percentages. Here too it is evident that later main-sequence spectral types in the binary produce lower diagnostics. As this is due to the shorter transit durations (from the lower stellar radii), giant and sub-giant binaries in blends would produce very high diagnostics that would be easily separable from exoplanets. The shaded regions in this figure are identical to those in Fig. 5. This figure also shows that a relatively high percentage of blends can be separated from exoplanets, especially those orbiting late spectral-type parent stars.

Incorporating an estimate of the primary radius improves the performance of the diagnostic. Figure 7 is similar to Figure 6, except that stellar radii are assumed to be known to within 20% (top) and 5% (bottom). For clarity, only the highest (F2/F2 binary) and the lowest (M3/M3 binary) of the 70% transit percentage contours are shown. Information on stellar radii affects the locations of the exoplanet regions so that central transits have a diagnostic close to one, within the limits of the errors, which is quite different from earlier figures. Moreover, the imprecision in the estimate of stellar radius affects the diagnostics of the blends as well. In this figure, the information on spectral type show that blends in which the “primary” is a late spectral type will be the easiest to separate from exoplanets, while those involving the earliest spectral types will not gain much from the use of the diagnostic. To date, only about 12% of exoplanets discovered with either radial velocity or transits have been around F stars. This of course could be affected by the choice of stars in radial velocity searches.

4. Conclusions

We have devised an exoplanet diagnostic η and shown that it can be an effective tool in choosing transit candidates worthy of follow-up observation. Using our diagnostic, many eclipsing binary stars, especially those involving giants, and blends can be excluded from further consideration. Specifically, we suggest that OGLE-TR-33 is unlikely to be planetary, while our analysis indicated that OGLE-TR-10 had a high likelihood of being planetary before it was confirmed (Bouchy et al. 2004). Estimates of stellar radii improve the performance of the diagnostic, giving it an even greater ability to identify the events that are non-exoplanetary in origin. The diagnostic will be particularly useful for bodies (such as hot Jupiters) that have circular orbits. The addition of eccentricity to the analysis leads to an increased spread in the diagnostic, but does not critically impair the method. Transits are

more likely to occur in portions of an eccentric orbit where v_t exceeds v_{circular} , leading to a reduction in the average diagnostic for exoplanetary systems with a given period. Overall, we encourage the use of this diagnostic tool in the search for exoplanets via transits to reduce the large numbers of candidates that require resource-consuming follow-up observations.

REFERENCES

Alonso, R., Brown, T. M., Torres, G., Latham, D. W., Sozzetti, A., Mandushev, G., Belmonte, J. A., Charbonneau, D., Deeg, H. J., Dunham, E. W., O'Donovan, F. T., & Stefanik, R. P. 2004, *ApJ*, 613, 153

Bouchy, F., Pont, F., Santos, N. C., Melo, C., Mayor, M., Queloz, D., & Udry, S. 2004, *A&A*, 421, L13

Pont, F., Bouchy, F., Queloz, D., Santos, N. C., Melo, C., Mayor, M., & Udry, S. 2004, *A&A*, 426, L15

Brown, T. M., Charbonneau, D., Gilliland, R. L., Noyes, R. W., & Burrows, A. 2001, *ApJ*, 552, 699

Claret, A. 2000, *A&A*, 363, 1081

Cox, A. N. 2000, in *Allen's Astrophysical Quantities* (New York: AIP), 355-357

Drake, A. J. 2003, *ApJ*, 589, 1020

Halbwachs, J. L., Mayor, M., & Udry, S. 2004, astro-ph/0410732, to appear in *A&A*

Konacki, M., Torres, G., Jha, S., & Sasselov, D. D. 2003, *Nature*, 421, 507

Konacki, M., Torres, G., Sasselov, D. D., & Jha, S. 2004, astro-ph/0412400, to appear in *ApJ*

Sackett, P. 1999, in *Planets Outside the Solar System: Theory and Observations (NATO-ASI)*, ed. J. M. Mariotti & D. Alloin (Dordrecht: Kluwer), 189

Sirko, E. & Paczyński, B. 2003, *ApJ*, 592, 1217

Seager, S. & Mallén-Ornelas, G. 2003, *ApJ*, 585, 1038

Tingley, B. 2004, *A&A*, 425, 1125

Torres, G., Konacki, M., Sasselov, D. D., & Jha, S. 2004, *ApJ*, 614, 979

Udalski, A., Paczyński, B., Żebruń, K., Szymański, M., Kubiak, M., Soszyński, I., Szewczyk, O., Wyrzykowski, Ł., & Pietrzyński, G. 2002a, *AcA*, 52, 1

Udalski, A., Paczyński, B., Żebruń, K., Kubiak, M., Soszyński, I., Szewczyk, O., Wyrzykowski, Ł., & Pietrzyński, G. 2002b, *AcA*, 52, 115

Udalski, A., Szewczyk, O., Żebruń, K., Pietrzynski, G., Szymański, M., Kubiak, M., Soszyński, I., & Wyrzykowski, Ł. 2002c, *AcA*, 52, 317

Udalski, A., Pietrzyński, G., Szymański, M., Kubiak, M., Żebruń, K., Soszyński, I., Szewczyk, O., & Wyrzykowski, Ł. 2003, *AcA*, 53, 133

Udalski, A., Szymański, M., Kubiak, M., Pietrzyński, G., Soszyński, I., Żebruń, K., Szewczyk, O., & Wyrzykowski, Ł. 2004, *AcA*, 54, 313

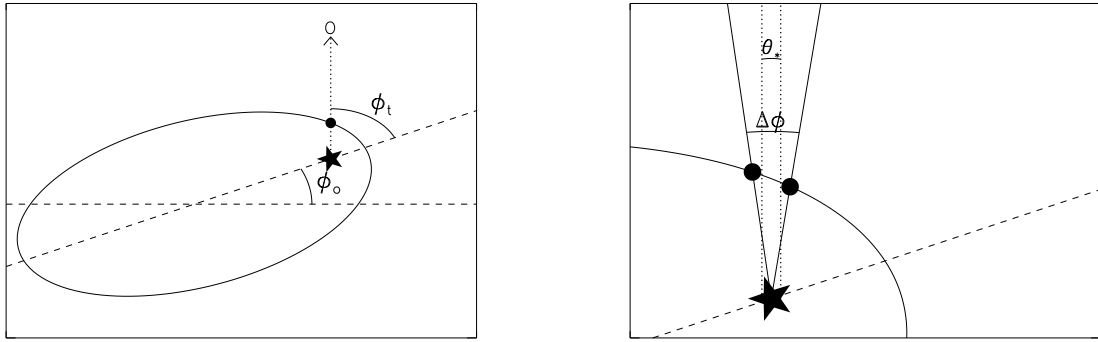


Fig. 1.— Geometry of an observed transit and definitions of relevant angles used in the text. $\frac{\pi}{2} - \phi_o$ is the angle between the semi-major axis of the orbit and the line of sight. ϕ_t is the eccentric angle of transit center relative to ϕ_o . θ_* is the angular size of the parent star as measured by a distant observer. The eccentric angle $\Delta\phi$ is measured between first contact and last contact of the transit.

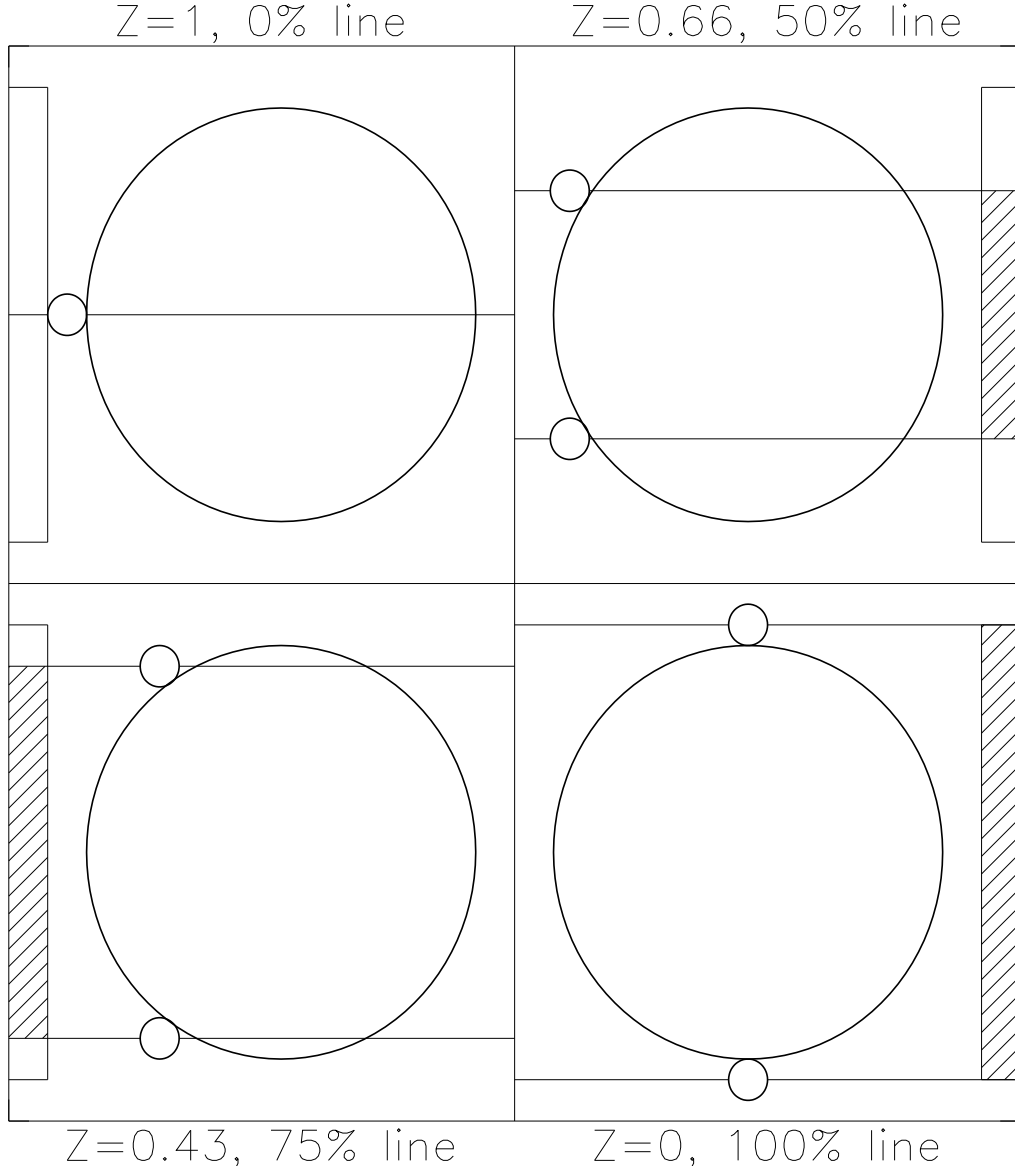


Fig. 2.— A visualization of the geometric interpretation of Z . This figure demonstrates how Z relates to the path of an exoplanets across the disk and how that, in turn, relates to the percentage of all possible transits (assuming random orbital orientations) that will exhibit a Z greater than or equal to a chosen Z . The large circles represent the parent stars while the small ones are exoplanets. The straight lines across the disks are the orbital paths of the exoplanets, which correspond to the Z s shown at the top of the figure. The boxes at the outside edge of the figure show what percentage of all possible transits (assuming random orbits) that have a Z greater than the listed Z . This percentage (which will be referred to later as transit percentage (P_t)) is related to Z by $P_t = \sqrt{1 - Z^2}$. The upper-left hand figure shows a central transit (with $Z = 1$ and the bottom-right shows the other extreme, the narrowest of grazing transits, corresponding to $Z = 0$). The other two figures show in-between cases, demonstrating how transit duration (proportional to the crossing time across the disk of the star from first contact to last) varies with Z .

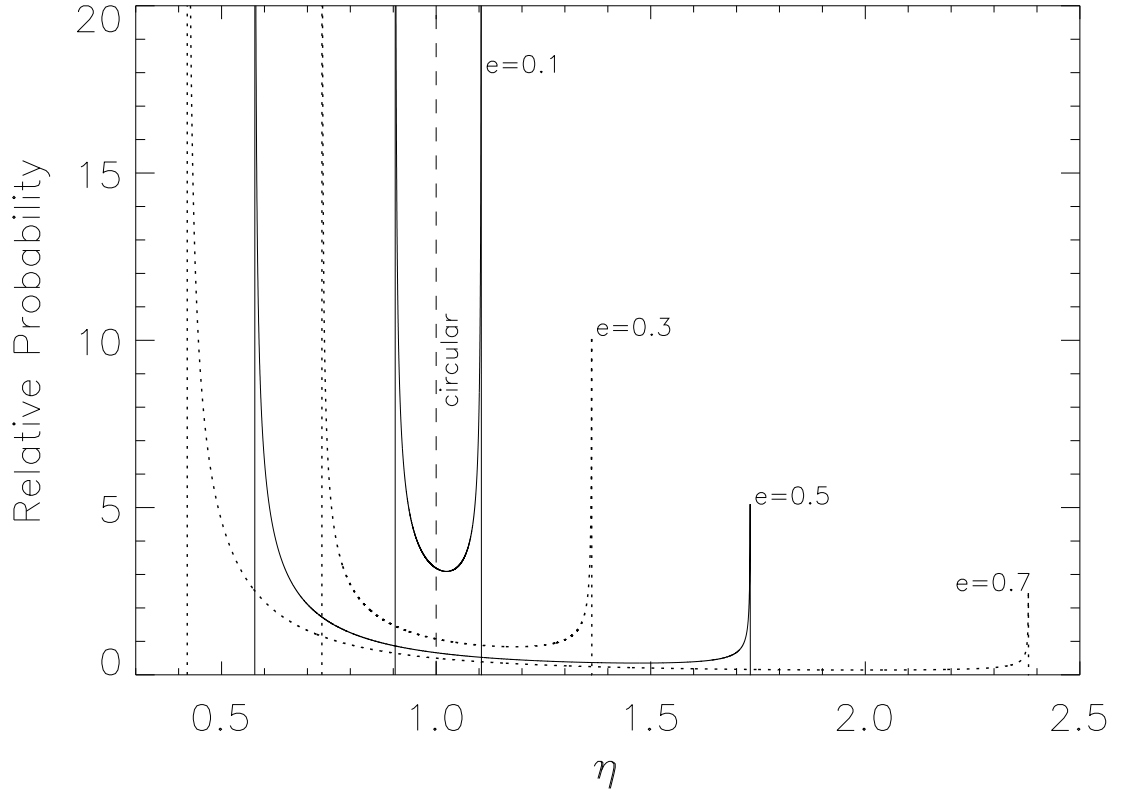


Fig. 3.— The effect of eccentricity on the spread of possible diagnostics η for a central transit with a fixed period. The labels on each line represent the eccentricity and the dashed line represents the exoplanet diagnostic for a circular orbit. Notice how the spread increases as the eccentricity increases, but the probability of a transit having a large diagnostic decreases significantly ($\propto \sqrt{1 - e^2}$ as demonstrated in Eq. 18). As the diagnostics shown are only for central transits, they therefore represent the maximum possible observed diagnostic for the given parameters.

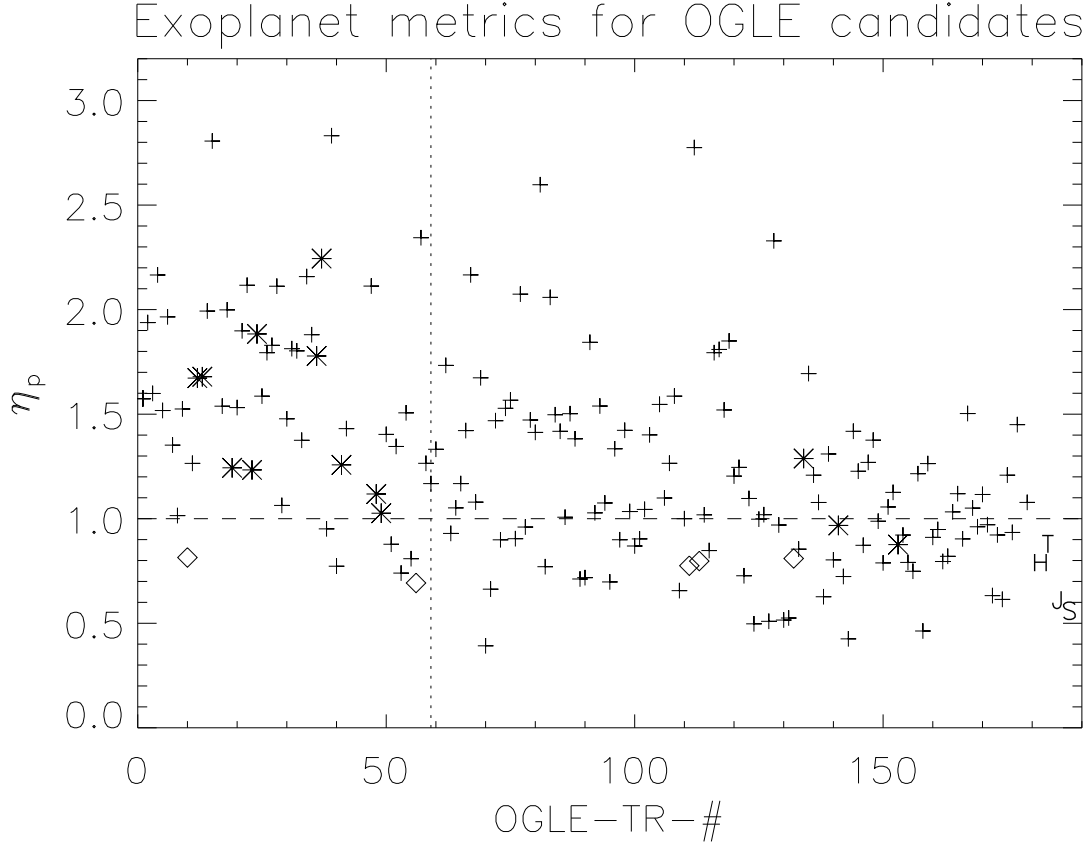


Fig. 4.— The exoplanet diagnostic plotted against OGLE transit candidate identifiers, assuming an exoplanetary radius of $1R_J$. The horizontal dashed line represents the cutoff below which any exoplanets in the sample should fall. The vertical dotted line shows the dividing line between the subset that is completely followed-up (left side) and those for which the analysis is incomplete (right side). The crosses represent candidates that are either binary stars or unclassified, while the diamonds are the known exoplanets in the sample. The observed transit of HD209458 (Brown et al. 2001) is marked with an “H” and the observed transit of TrES-1 Alonso et al. (2004) marked with a “T”. A theoretical central Jupiter transit is marked with a “J” and a theoretical central Saturn transit is marked with an “S”. Note that the exoplanets (both known and modeled) lie well below the cut-off line given by our criterion $\eta \leq 1$. Lastly, the observed slope in this figure is not real; it is likely indicative of the OGLE group’s increasing ability to remove eclipsing binaries from the candidate list. The data used to create this figure can be found in Table 1.

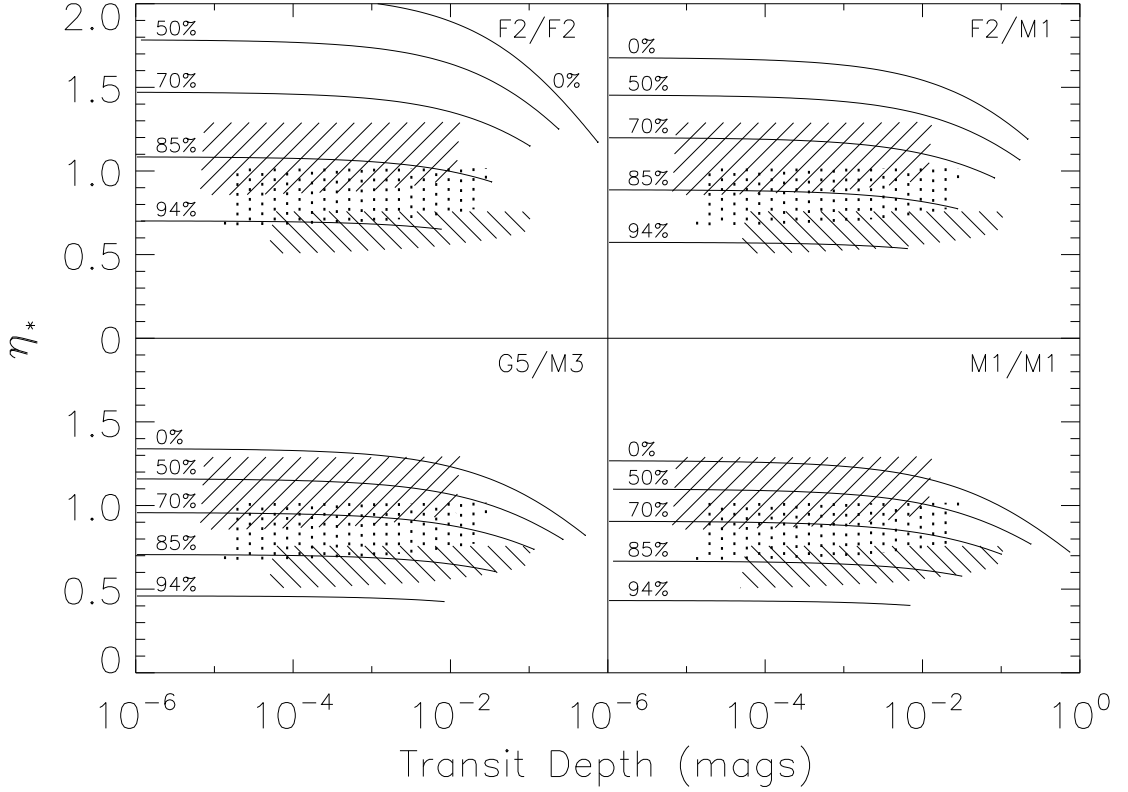


Fig. 5.— The exoplanet diagnostic for different blended binary systems at transit percentages (as described in Fig. 2) as a function of observed transit depth, assuming that the stellar radius for the “primary” (the constant component for a blend, the parent star for an exoplanet) is unknown and therefore using R_{\odot} to calculate η_{\star} . The lines depict the evolution of the diagnostic of a series of blends as increasingly more light from a unvarying third component is added to the light from an eclipsing binary to reduce the transit depth. The lines are labeled by the transit percentage. For comparison, shaded regions indicate diagnostics for exoplanets ranging in size from $1.5R_J$ down to R_{Mercury} around F2 stars (highest), the Sun (middle) and an M3 star (bottom), assuming that R_{\star} is known when calculating η_{\star} . A shaded region is bounded on top by modeled central transits and on the bottom by modeled transits with a transit percentage of 75%, or $Z = \sqrt{1 - 0.75^2} = 0.66$. Note that the majority of blends are not in regions where exoplanets would be found for larger stars. True grazing binaries without blending fall where lines end on the right.

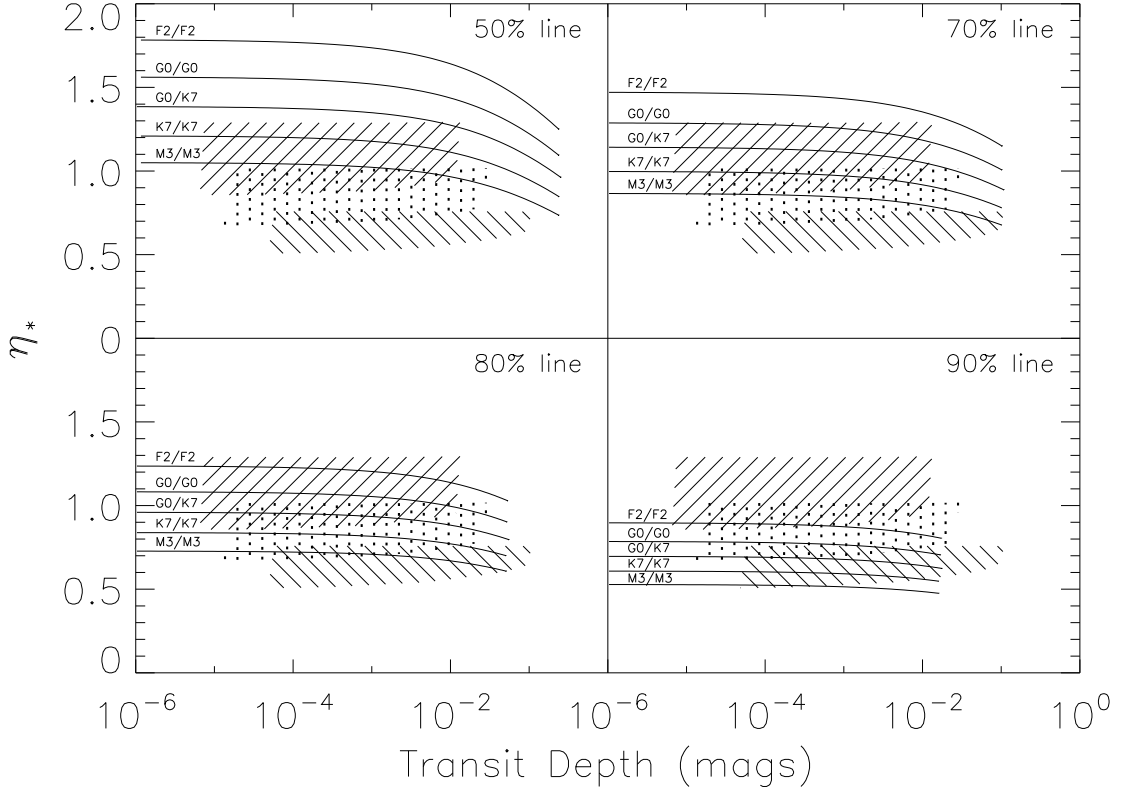


Fig. 6.— Similar to Fig. 5, this figure shows how the diagnostics of blends for different transit percentages and binary spectral types compare to those for exoplanets, again assuming $R_\star = R_\odot$. The label for each line indicates the spectral types modeled, while the label for each subsection of the figure corresponds to the inclination. The shaded regions are as described in Fig. 5. This figure demonstrates that the diagnostic is effective for separating most, but certainly not all, blends from exoplanets. The confusion will be most acute for those exoplanets around the more massive stars included in the study.

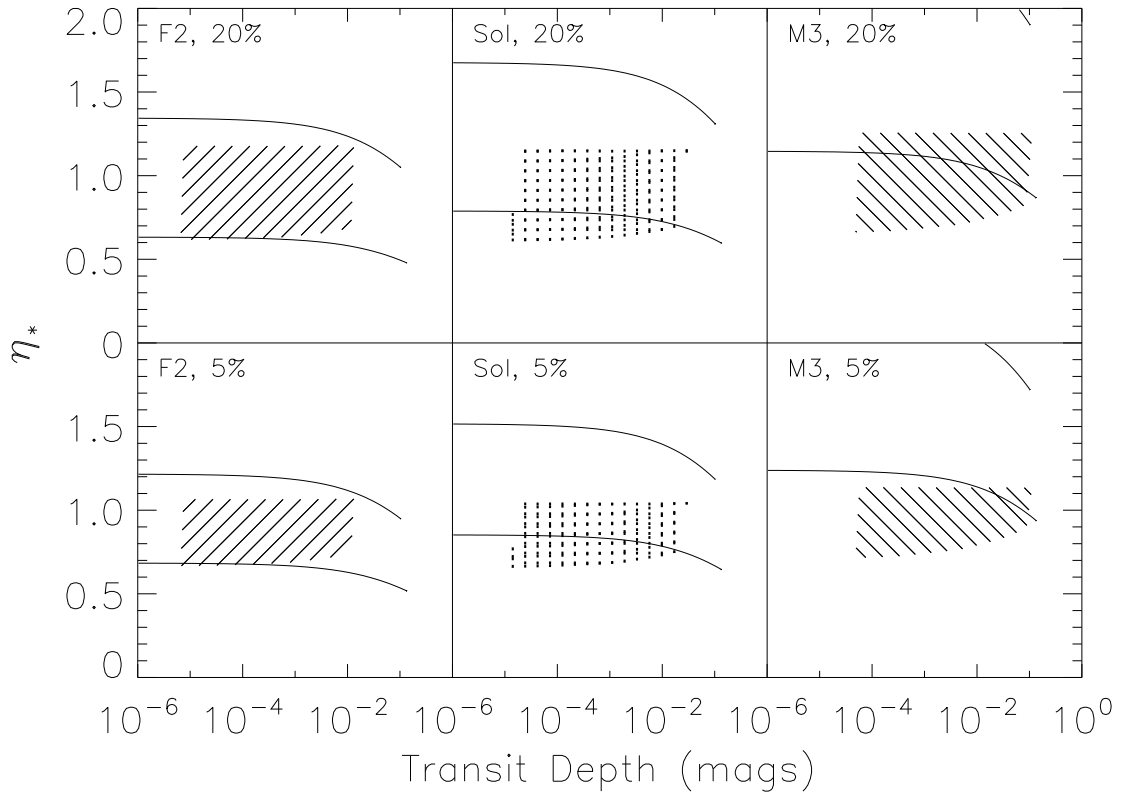


Fig. 7.— Similar to Fig. 6, except for the fact that stellar radius for the “primary” is known to either 20% (top) or 5% (bottom) precision when calculating η_* , the “primary” being the constant component for blends and the parent star for exoplanets. Only 70% contours for a blend with a F2/F2 (highest modeled diagnostics) and an M3/M3 (lowest modeled diagnostics) eclipsing component are shown for clarity. The shades regions show the range of diagnostics for exoplanets (75% transit percentages) around the stars of the listed spectral types where the radius is known to the listed precision. Notice how the shades regions cover approximately the same range in diagnostics in all the figures, though narrower for the bottom three figures due to the higher precision in the measured “primary” radius. Notice also how exoplanets are easier to separate from blends for later spectral types.

Table 1. Transit Parameters and Diagnostics for the OGLE candidates

OGLE-TR-#	Period (days)	Duration (days)	Depth(mags)	η_p
1	1.600	0.117	0.043	1.02
2	2.813	0.209	0.019	1.54
3	1.189	0.129	0.019	1.27
4	2.618	0.174	0.065	2.06
5	0.808	0.090	0.043	1.08
6	4.548	0.197	0.053	1.78
7	2.717	0.126	0.034	1.38
8	2.715	0.088	0.048	0.99
9	3.268	0.140	0.048	1.61
10	3.101	0.091	0.019	0.82
11	1.615	0.090	0.053	1.07
12	5.772	0.195	0.038	1.01
13	5.853	0.208	0.030	1.49
14	7.797	0.264	0.034	2.09
15	4.874	0.337	0.026	2.56
16	2.138	0.451	0.026	2.21
17	2.317	0.136	0.034	1.60
18	2.228	0.165	0.043	1.27
19	5.282	0.126	0.065	1.02
20	4.283	0.147	0.059	1.31
21	6.892	0.229	0.043	2.70
22	4.275	0.180	0.084	2.35
23	3.286	0.109	0.059	1.17
24	5.282	0.199	0.053	1.77
25	2.218	0.135	0.038	1.44
26	2.538	0.148	0.053	1.39
27	1.714	0.155	0.026	1.75
28	3.405	0.193	0.053	2.06
29	2.715	0.092	0.048	0.99
30	2.365	0.128	0.038	1.50
31	1.883	0.154	0.030	1.71

Table 1—Continued

OGLE-TR-#	Period (days)	Duration (days)	Depth(mags)	η_p
32	1.343	0.133	0.034	0.93
33	1.953	0.115	0.034	1.34
34	8.581	0.273	0.048	2.13
35	1.259	0.139	0.030	1.10
36	6.251	0.194	0.059	1.80
37	5.719	0.275	0.030	2.20
38	4.101	0.094	0.048	1.14
39	0.815	0.181	0.030	1.00
40	3.430	0.083	0.026	0.76
41	4.517	0.153	0.022	1.46
42	4.161	0.149	0.038	1.80
47	2.335	0.214	0.019	1.73
48	7.225	0.159	0.022	1.00
49	2.690	0.095	0.034	1.03
50	2.248	0.114	0.048	1.25
51	1.748	0.071	0.034	0.85
52	1.325	0.099	0.034	1.28
53	2.905	0.070	0.034	0.84
54	8.162	0.215	0.026	1.35
55	3.184	0.091	0.019	1.00
56	1.211	0.062	0.013	0.64
57	1.674	0.197	0.026	1.72
58	4.345	0.142	0.030	1.76
59	1.497	0.095	0.026	1.02
60	2.308	0.140	0.016	1.21
61	4.268	0.474	0.030	3.33
62	2.601	0.155	0.038	1.83
63	1.066	0.083	0.011	0.85
64	2.717	0.108	0.022	0.93
65	0.860	0.074	0.034	1.01
66	3.514	0.131	0.053	1.27

Table 1—Continued

OGLE-TR-#	Period (days)	Duration (days)	Depth(mags)	η_p
67	5.279	0.229	0.053	1.97
68	1.288	0.081	0.030	1.02
69	2.337	0.145	0.038	1.28
70	8.040	0.048	0.053	0.36
71	4.187	0.079	0.022	0.69
72	6.854	0.173	0.048	1.38
73	1.581	0.070	0.034	0.88
74	1.585	0.122	0.030	0.78
75	2.642	0.144	0.034	1.58
76	2.126	0.086	0.022	0.70
77	5.455	0.269	0.022	1.90
78	5.320	0.115	0.030	1.05
79	1.324	0.111	0.030	1.18
80	1.807	0.137	0.016	1.25
81	3.216	0.282	0.022	1.86
82	0.764	0.047	0.034	0.76
83	1.599	0.191	0.016	0.78
84	3.113	0.129	0.059	1.41
85	2.114	0.113	0.048	1.57
86	2.777	0.082	0.065	0.93
87	6.606	0.167	0.059	1.52
88	1.250	0.099	0.034	1.37
89	2.289	0.078	0.013	0.73
90	1.041	0.054	0.022	0.55
91	1.579	0.136	0.043	1.52
92	0.978	0.066	0.038	0.95
93	2.206	0.153	0.019	1.40
94	3.092	0.099	0.043	1.05
95	1.393	0.059	0.019	1.16
96	3.208	0.125	0.043	1.08
97	0.567	0.059	0.016	0.95

Table 1—Continued

OGLE-TR-#	Period (days)	Duration (days)	Depth(mags)	η_p
98	6.398	0.176	0.034	1.52
99	1.102	0.071	0.034	0.88
100	0.826	0.062	0.019	0.82
101	2.361	0.078	0.038	0.75
102	3.097	0.116	0.019	0.88
103	8.216	0.175	0.048	1.55
104	6.068	0.413	0.053	1.94
105	3.058	0.159	0.026	1.05
106	2.535	0.110	0.022	1.09
107	3.189	0.113	0.053	1.26
108	4.185	0.158	0.048	1.49
109	0.589	0.052	0.008	0.85
110	2.848	0.100	0.026	0.90
111	4.016	0.094	0.019	0.78
112	3.879	0.346	0.016	2.45
113	1.432	0.061	0.030	0.80
114	1.712	0.086	0.026	0.88
115	8.346	0.102	0.059	0.38
116	6.064	0.184	0.077	1.87
117	5.022	0.213	0.030	1.52
118	1.861	0.143	0.019	1.65
119	5.282	0.210	0.038	1.84
120	9.165	0.142	0.077	1.23
121	3.232	0.105	0.071	1.28
122	7.268	0.107	0.019	0.78
123	1.803	0.126	0.008	1.12
124	2.753	0.061	0.011	0.53
125	5.303	0.145	0.013	1.01
126	5.110	0.129	0.022	0.95
127	1.927	0.055	0.011	0.60
128	7.391	0.360	0.016	2.26

Table 1—Continued

OGLE-TR-#	Period (days)	Duration (days)	Depth(mags)	η_p
129	5.740	0.116	0.034	0.76
130	4.830	0.061	0.028	0.49
131	1.869	0.056	0.011	0.58
132	1.689	0.084	0.011	0.80
133	5.310	0.099	0.034	0.81
134	4.537	0.186	0.011	0.87
135	2.573	0.177	0.019	1.56
136	3.115	0.140	0.016	1.22
137	2.537	0.101	0.030	0.96
138	2.645	0.069	0.016	0.86
139	2.534	0.122	0.030	0.96
140	3.393	0.076	0.043	0.79
141	5.678	0.132	0.019	0.74
142	3.062	0.070	0.034	0.56
143	3.349	0.065	0.006	0.39
144	2.445	0.127	0.034	1.24
145	2.741	0.131	0.019	1.21
146	2.944	0.079	0.043	0.95
147	3.841	0.136	0.030	0.99
148	1.432	0.114	0.022	1.25
149	4.551	0.116	0.026	0.86
150	2.073	0.107	0.005	0.93
151	1.483	0.089	0.022	1.01
152	3.730	0.133	0.019	1.12
153	4.395	0.098	0.030	0.85
154	3.669	0.119	0.013	0.90
155	5.277	0.130	0.008	1.01
156	3.583	0.076	0.034	0.64
157	5.868	0.139	0.043	0.91
158	6.384	0.065	0.019	0.39
159	2.126	0.106	0.038	1.26

Table 1—Continued

OGLE-TR-#	Period (days)	Duration (days)	Depth(mags)	η_p
160	4.901	0.146	0.008	0.72
161	2.747	0.135	0.006	1.03
162	3.758	0.107	0.011	0.66
163	0.946	0.053	0.034	0.80
164	2.681	0.109	0.019	0.95
165	2.891	0.101	0.043	1.33
166	5.219	0.136	0.011	0.88
167	5.261	0.192	0.022	0.65
168	3.650	0.135	0.013	0.67
169	2.768	0.103	0.019	1.28
170	4.136	0.127	0.026	1.22
171	2.091	0.081	0.038	0.99
172	1.793	0.078	0.006	0.74
173	2.605	0.097	0.019	0.49
174	3.110	0.071	0.016	0.74
175	1.488	0.105	0.019	1.15
176	3.404	0.103	0.022	0.87
177	5.643	0.168	0.038	0.81
HD209458	3.524	0.1298	0.0167	0.85
TrES-1	3.030	0.1250	0.023	0.94
Jupiter	4346	1.236	0.010	0.67
Saturn	10760	1.675	0.0073	0.62

Note. — Note that the durations were measured estimated using a simple matched filter code from the data available on the OGLE website, [http://bulge.princeton.edu/ ogle/](http://bulge.princeton.edu/ogle/).